

論文 / 著書情報  
Article / Book Information

Title	Suffusion-induced change in spatial distribution of fine fractions in embankment subjected to seepage flow
Authors	Kazuki Horikoshi, Akihiro Takahashi
Citation	Soils and Foundations, Vol. 55, Issue 5, pp. 1293-1304
Pub. date	2015, 10
DOI	<a href="http://dx.doi.org/10.1016/j.sandf.2015.09.027">http://dx.doi.org/10.1016/j.sandf.2015.09.027</a>
Creative Commons	See next page.
Note	This file is author (final) version.

# License



Creative Commons: CC BY-NC-ND

1 **Title:**  
2 **Suffusion-induced change in spatial distribution of fine fractions in embankment**  
3 **subjected to seepage flow**

4

5 **Author 1:**

6 Kazuki Horikoshi

7 Graduate student, Department of Civil Engineering, Tokyo Institute of Technology, Tokyo, Japan

8

9 **Author 2, Corresponding author:**

10 Akihiro Takahashi

11 Professor, Department of Civil Engineering, Tokyo Institute of Technology, Tokyo, Japan

12

13 **Full contact details of corresponding author.**

14 Akihiro Takahashi (Author 2)

15 2-12-1-M1-3 Oh-okayama, Meguro, Tokyo 152-8552

16 Tel: 03-5734-2593, E-mail: takihiro@cv.titech.ac.jp

17

18 **Soils and Foundations, 55(5), 1293-1304, 2015**

19 **Original URL:**

20 **<http://dx.doi.org/10.1016/j.sandf.2015.09.027>**

21

22 **Abstract**

23 Suffusion describes the phenomenon whereby finer particles are eroded through the voids of coarse  
24 particles by the seepage flow. This may cause the deterioration of the hydraulic structure and, in the  
25 worst case, result in the failure of the hydraulic structure. The suffusion process is presented in this  
26 paper in an embankment under transient and steady seepage conditions. A series of physical model  
27 tests on seepage-induced suffusion on a small-scale model embankment is performed under constant  
28 boundary head conditions. A binary mixture, consisting of two Silica sands (Silica sands Nos. 3 and  
29 8), which is categorized as “internally unstable material” by several previous criteria for the  
30 seepage-induced internal stability, is used for the model embankment. The cumulative eroded soil  
31 mass and the discharged rate of water are recorded during the seepage tests. The spatial extent of the  
32 variation in erosion-induced fines contents is discussed through sieve analyzes on subdivided areas  
33 of the model embankment after seepage testing. The test results reveal that a decrease in fines  
34 propagates along the phreatic surface from downstream in the embankment. Below the phreatic  
35 surface, the eroded fines not only move laterally by the seepage flow, but also vertically due to the  
36 gravitational force, and are deposited in the foundation. This deposition of the fines results in the  
37 expansion of the fine-rich region in the foundation and causes a decrease in the permeability of the  
38 whole embankment.

39  
40 Keyword: suffusion; internal erosion; seepage; physical model tests

41  
42 **International Geotechnical Classification System**

43 E07

44

45

46 1. Introduction

47 Erosion induced by seepage inside embankments is called internal erosion. This phenomenon is  
48 known to be one of the causes of the deterioration of hydraulic structures and, in severe cases,  
49 triggers the failure of the structures (e.g., Foster et al., 2000; Richards and Reddy, 2007; Fry et al.,  
50 2012). Ground disasters caused by this phenomenon have not only occurred in hydraulic structures,  
51 but also in reclaimed land (Khomeenko, 2006; Kuwano et al., 2012).

52

53 Types of internal erosion include concentrated leak erosion, contact erosion, backward erosion, and  
54 suffusion (Fry, 2012; Fell and Fry, 2013). Concentrated leak erosion is driven by the seepage flow in  
55 the opening (crack or cavity). It detaches particles from the sides of the opening. Contact erosion is  
56 the erosion of particles at the interface between fine and coarse layers due to a quasi- horizontal  
57 groundwater flow. Backward erosion describes the erosion of soil particles at the exit end of a  
58 seepage path, such as leaking through the downstream surface due to a high exit velocity or  
59 hydraulic gradient. Suffusion describes the phenomenon whereby finer particles are eroded through  
60 the voids between the coarse particles by the seepage flow. It is also described as “a special case of  
61 backward erosion peculiar to gap-graded soil” (Richards and Reddy, 2014). This paper focuses on  
62 the suffusion phenomenon.

63

64 The process of dam failure by internal erosion and piping is classified into four phases: the initiation  
65 of erosion, the continuation of erosion, the progression to form a pipe, and the formation of a breach  
66 (Foster and Fell, 1999). Foster and Fell (1999) described this erosion process by detailed event trees.  
67 Some of the steps of this process show how failure initiated due to suffusion in an embankment or its  
68 foundation; this is the target of the present study.

69

70 Moffat et al. (2011) defined suffusion as the phenomenon whereby “the finer fraction of an internally  
71 unstable soil moves within the coarser fraction without any loss of matrix integrity or change in total  
72 volume,” whereas with suffosion, “particle migration yields a reduction in total volume and a  
73 consequent potential for collapse of the soil matrix”. In this paper, the widely accepted term  
74 “suffusion” is used.

75

76 Suffusion develops in the first two phases, namely, the initiation of erosion and the continuation of  
77 erosion, in the failure scenarios initiated by suffusion. This phenomenon is a potential risk to the  
78 long-term stability of hydraulic structures over a period of years. During these phases, the  
79 performance of a hydraulic structure, e.g., the hydraulic and mechanical characteristics, might  
80 deteriorate progressively. On the other hand, the time scale for the third and fourth phases related to  
81 piping, namely, the progression to form a pipe and the formation of a breach, are relatively short,  
82 compared with the time scale for the first two phases. In other words, the hydraulic structure is in the  
83 phases of the initiation or the continuation of erosion for most of its service life. Therefore, this study

84 focuses on the suffusion development phase and includes the initiation of erosion and the  
85 continuation of erosion phases.

86

87 For the initiation of erosion phase in the failure process of embankment dams, many research works  
88 have been conducted on suffusion and internal instability based on one-directional upwards or  
89 downwards seepage experiments; the initiation of this phenomenon depends on the particle size  
90 ratio between the finer fraction and the coarse fraction (e.g., Honjo et al., 1996; Terzaghi, 1939), the  
91 particle size distribution (e.g., Kenney and Lau, 1985; Li and Fannin, 2008; Wan and Fell, 2008;  
92 Chang and Zhang, 2013; Moraci et al., 2014), the particle shape (Marot et al., 2012), the confining  
93 pressure (e.g., Bendahmane et al., 2008; Moffat and Fannin, 2011), the hydraulic gradient (e.g.,  
94 Skempton and Brogan; 1994, Sterpi, 2003), the flow velocity (Perzmaier et al., 2007), and the  
95 seepage angle (Richards and Reddy, 2012, 2014), among other factors. Richards and Reddy (2014)  
96 suggested a methodology based on kinetic energy to predict suffusion and the backward erosion  
97 initiation potential and performed analyses of the factors of safety against these phenomena for a  
98 homogenous embankment model with a foundation.

99

100 For the continuation of erosion phase, the development of erosion depends on the presence or  
101 absence of an adequate filter or transition zone (Foster and Fell, 1999). Moffat et al. (2011) showed  
102 the spatial and temporal progression of seepage-induced internal instability, which included suffusion  
103 and suffusion from the initiation to the progression phases in a one-dimensional seepage field. They  
104 observed the conditions of the specimen through a transparent wall and measured the local hydraulic  
105 gradient in the specimen. Luo et al. (2012) described the evolution of suffusion in pore scale as: “fine  
106 particles migration-pores clogging-pushing out clogging pores-fine particles remigration.” These  
107 observations were made in the laboratory in a relatively short period, i.e., days. However, the time  
108 scale for the initiation and the continuation of suffusion phases in a real embankment or foundation is  
109 very slow, i.e., from months to years (Fell et al., 2003).

110

111 Most of the above-mentioned suffusion studies focused on the phenomenon in a uniform  
112 one-dimensional seepage field, while the seepage flow in a real structure is more complex and so is  
113 the suffusion progress. However, there are few studies which consider the effect of the geometry of a  
114 real structure on suffusion in the initiation and the continuation phases. The laboratory experiments  
115 of Lindow et al. (2009) suggested that the failure mechanism due to seepage is dependent on the  
116 slope angle. Sterpi (2003), Cividini and Gioda (2004) and Cividini et al. (2009) carried out finite  
117 element analyses to examine the spatial and temporal distributions of fines under seepage with a  
118 phreatic surface by modifying the erosion model proposed by Sterpi (2003). Uzuoka et al. (2012) and  
119 Zhang et al. (2013, 2014) demonstrated the temporal change in fines within the “geometry” of the  
120 embankment by means of numerical simulations.

121

122 Experimental studies on internal erosion have been conducted for large-scale contact erosion  
123 (Beguin et al., 2012). To the authors' knowledge, studies based on physical model tests for suffusion  
124 are limited (Saito et al., 2012). Saito et al. (2012) provided eight hours of water supply, 16 h of  
125 drainage and 180 repetitions to a physical model, which was made of pit sand to imitate a levee.  
126 After seepage testing, the fines content was examined at four locations within the model levee.

127

128 In this paper, a series of physical model tests is performed on a small-scale model to examine the  
129 seepage-induced suffusion process in an embankment during the phases of the initiation and the  
130 continuation of erosion.

## 131 2. Experimental apparatus and procedure

### 132 2.1 *Material*

133 To simplify the phenomenon, a mixture of fine and coarse fractions, namely, a gap-graded soil, is  
134 used for the model. This type of gap-graded soil exists in the glacial tills of Canada and New Zealand,  
135 but sometimes is used as material for filling. To use a dredged soil as a fill material, its workability is  
136 improved by mixing in cement or pit sand. Typically, the latter is a gap-graded soil. Although use of  
137 such a material can exaggerate the test results, it allows (a) easy distinction between the base and the  
138 erodible materials and (b) easy observation of the fines migration in a short period.

139

140 Based on the works by Ke and Takahashi (2012, 2014), Silica sands Nos. 3 and 8 are used as the  
141 model materials. Silica sand No. 3 is applied to model the soil skeleton, while Silica sand No. 8 is  
142 applied as the erodible fines particles in the voids of the coarse skeleton. Hereafter, Silica sand No. 8  
143 is referred to as fines for simplicity, even though Silica sand No. 8 is not strictly classified as fines by  
144 the Japanese Industrial Standards (JIS). The chosen fines content of the mixture is 15%. The particle  
145 size distribution curves for each type of sand are shown in Fig. 1, while the mixture and the basic  
146 properties of the mixture material are shown in Table 1.

147

148 According to several criteria on seepage-induced internal stability (Chang and Zhang, 2013; Wan and  
149 Fell, 2008; Li and Fannin, 2008), the mixture used in this study is categorized as “Internally unstable  
150 material” and it is vulnerable to suffusion if seepage takes place. The calculated critical hydraulic  
151 gradient for zero effective stress is 1.0 according to Terzaghi's equation. Ke and Takahashi (2012)  
152 performed a series of one-dimensional upward seepage tests on a similar mixture with fines contents  
153 of 14.3, 16.7, 20, and 25%. Their critical gradient for suffusion,  $i_{sc}$ , was linearly correlated with the

154 fines content,  $FC$  ( $i_{sc} = -0.0037FC + 0.302$ ,  $R^2 = 0.997$ ). From this linear relationship, the  
155 expected critical gradient against suffusion for the mixture used in this study (15% fines content) is  
156 0.25.

157

158 Permeability tests are conducted on specimens with varying fines contents ( $FC = 2.5\text{--}30.0\%$ ) under a  
159 constant void ratio of the coarse skeleton (void ratio of the coarse skeleton,  $e_s = 0.885$ ; relative  
160 density of the coarse skeleton,  $Dr_s = 40\%$ ) in accordance with JIS and Japanese Geotechnical Society  
161 (JGS) standards. In the tests, a small hydraulic gradient is imposed so that suffusion does not occur  
162 during the tests. Fig. 2 shows the relationship between hydraulic conductivity and the fines contents.  
163 In physical model tests, described later, the model embankment is made of partially saturated soil  
164 containing tap water. For these reasons, permeability tests are conducted on (a) soil that has been  
165 partially saturated with tap water and (b) soil that has been fully saturated with deaired water. Fig. 2  
166 indicates that the hydraulic conductivity of a specimen without deairing is lower than that of a fully  
167 saturated one. It should also be noted that, even at the same fines content, the packing of the fines  
168 may not be the same for these two conditions because the position of the fines in the voids of the  
169 coarse skeleton are different depending on whether or not air bubbles exist in the voids.

## 170 2.2 *Experimental apparatus*

171 The embankment models are made in a steel box with inner dimensions of  $500\text{ mm} \times 150\text{ mm} \times 350$   
172  $\text{mm}$ , as shown in Fig. 3(a). The box has two tanks on both sides, namely the “water supply tank” and  
173 the “drainage tank.” The vertical sidewalls between the tank and the embankment model contain a  
174 metal mesh so that only water and fines less than  $0.25\text{ mm}$  can flow through them. By pouring water  
175 into the water supply tank, the seepage flow in the ground can be modeled. The boundary heads  
176 reach  $190\text{ mm}$  and  $40\text{ mm}$  at the upstream and downstream sides, respectively, in around  $30\text{--}40\text{ min}$   
177 for all cases. Seepage water from the model embankment eventually passes through the drainage  
178 tank and finally discharges from the outlet. The drainage tank has two holes, one is to discharge the  
179 eroded soil and some quantity of water (a small hole located at a level of  $0\text{ mm}$ ) and the other is to  
180 maintain a constant head (a large hole located at a level of  $40\text{ mm}$ ).

181

182 As shown in Fig. 3(b), the discharged soil and water flow into a small container via an aluminum  
183 angle. The small container is filled with water to a constant level and is located near the steel box.  
184 Eroded fines are collected in a bowl that is suspended on wires under the water inside the small  
185 container. To prevent the outflow of fines to the outside of the bowl and to help the sedimentation of  
186 fines, the bowl is covered with filter paper on the side surface. The cumulative eroded mass is  
187 recorded automatically by a load cell (Kyowa Electronic Instruments Co., Ltd., LVS-2KA,  
188 measurable range:  $0\text{--}20\text{ N}$ ) connected to the wires. The calibration of the load cell is performed  
189 before each seepage test, and the mass balance is also checked by the amount of collected eroded soil  
190 after each test.

191

192 To prevent material separation during the preparation of the model embankment, the moist tamping  
193 method (Ladd, 1978) is employed. The soil is compacted in layers, with a thickness of  $20\text{ mm}$ , where

194 no sensors are located. The pore pressure transducers used here are SSK Micro Pressure Transducers  
195 P306V-01 (measurable range: 0–10 kPa). To avoid the formation of a concentrated water path along  
196 the wiring of the sensors, the pore pressure transducers are placed near the back side of the steel box.  
197 An effort is made to measure the pore water pressure properly. However, the response of the sensor  
198 output was not so sharp, i.e., full saturation of the sensors may not have been achieved, since the  
199 tests started from the state in which the model embankment was under partially saturated conditions  
200 with a small water content. Even so, the sensor readings can be used to detect the arrival of water and  
201 to measure the changes in pore water pressure. The target dry density is  $1.560 \text{ g/cm}^3$  (void ratio,  $e =$   
202  $0.695$ ; relative density,  $Dr = 35\%$ ). The initial moisture content is 3.0%. After making the level  
203 ground, the model ground is scraped off with a shaped frame and formed to be a 260.5-mm-high  
204 embankment. To prevent the occurrence of a strong flow between the side wall and the model, a  
205 mixture of grease and silicon oil is put on the inside surface of the wall.

206

207 The model embankment is composed of two areas, the “foundation zone” and the “slope zone”  
208 (includes the “slope zone” and the “lower section of the crown”), as shown in Fig. 3(a). The  
209 foundation zone is an 80-mm-thick horizontal layer and the slope zone is an embankment with a  
210 slope of 1:1.8. According to a statistical survey of dam failures, this type of zoning, which has no  
211 zoning of materials or downstream filter, is most vulnerable to internal erosion (Foster and Fell,  
212 2001; Fry et al., 2012).

213

214 As far as the saturated seepage flow is concerned, the hydraulic gradient field in the model  
215 embankment is similar to a possible prototype, provided that the geometry of the embankment and  
216 the water head at the boundaries are consistent. However, if a phreatic water surface exists and  
217 internal erosion is involved, the following problems may arise and create limitations to this  
218 experiment: (1) the relative position of the phreatic surface in the small-scale model becomes higher  
219 than that in the prototype because the amount of capillary rise does not change with the model scale;  
220 and (2) the erosion-induced contractive deformation in the small-scale model can be diminished,  
221 since a soil becomes more dilative under small confining pressure. In addition to these problems, the  
222 confining pressure dependency of the fines loss is another concern. Ke and Takahashi (2014) carried  
223 out a series of one-dimensional downward seepage tests on a similar mixture with a fines content of  
224 35% under several levels of confining pressure and showed that the erosion potential decreases with  
225 an increasing confining pressure. Bendahmane et al. (2008) also showed a similar tendency for  
226 different internally unstable soil. Moffat et al. (2011), and Moffat and Fannin (2011) demonstrated  
227 that an increase in effective confining pressure would cause an increase in the critical hydraulic  
228 gradient for erosion. Tomlinson and Vaid (2000) investigated the effect of the confining pressure on  
229 the initiation of piping experimentally. Their results indicate that (a) the confining pressure has a  
230 certain influence on the internal stability if the ratio between the coarse and fines particles is not so  
231 large and (b) particle size ratio  $D_{15c}/d_{85f}$  is the most important parameter for the initiation of piping.

232 Considering these results, the stress level of an embankment may have little effect on suffusion.  
233 Therefore, useful data on the spatial changes in the fines content can be obtained by physical model  
234 tests in small-scale models.

### 235 2.3 Experiment procedures and conditions

236 In this study, the seepage flow stages of a transient seepage condition (first permeation to partially  
237 saturated model) and a steady seepage condition are reproduced using the above experimental system.  
238 First, the transport of fines in the above-mentioned stages is examined. By controlling the water level  
239 at the upstream boundary, the influence of repeated permeation on the spatial change in the fines in  
240 the embankment is also examined. Detailed test conditions and a conceptual diagram of the  
241 controlled water level at the upstream boundary are summarized in Table 2 and Fig. 4. The elapsed  
242 time is measured by the pouring of water into the water supply tank. The seepage flow in the  
243 embankment reaches a nearly steady condition in 30–40 min.

244  
245 A total of eight tests are conducted. *Case St1* is conducted to investigate the erosion during the first  
246 permeation stage (unsteady seepage condition) and the test is terminated as soon as the steady  
247 seepage condition is reached (Fig. 4). In the other cases (*Cases St20, St24, St48, and St280*), the  
248 seepage is continued for a prescribed time while keeping the water heads at the boundaries constant.

249  
250 *Cases St96RS4, St96RS8, and St280RS40* are carried out to assess the influence of the raising and the  
251 lowering of the phreatic surface on the spatial changes in the fines in the embankment. *Case St96RS4*  
252 consists of 1440 min of water supply, 1440 min of drainage, and four repetitions to the physical  
253 model. In *Case St96RS8*, repeated water penetrations are provided in eight cycles of 720 min. In this  
254 case, the value of the pore water pressure transducer at P1 in Fig. 3(a) shows a maximum head  
255 fluctuation of plus or minus 50 mm due to complications in the experimental system. In *Case*  
256 *St280RS40*, the repeated permeation times are random. The objective of *Case St280RS40* is to  
257 understand how the spatial distribution of the fines in the embankment is affected by the raising and  
258 the lowering of the phreatic surface. To exaggerate the spatial change in the fines, the raising and the  
259 lowering of the water level at the upstream are randomly conducted as many times as possible.

260  
261 During the seepage tests, the crown settlement is measured by displacement sensors. However, even  
262 in *Cases St280* and *StRS40*, which showed relatively large settlements, the maximum values were  
263 0.16 mm and 0.21 mm at the top of the slope and 0.06 mm and 0.24 mm at the center of the crown  
264 during the seepage tests. Compared with the initial model height of 260.5 mm, it can be said that the  
265 overall change in volume of the model embankment is negligible. Therefore, the volume change of  
266 the embankments is not considered in this study.

267  
268 After the seepage tests, a sieve analysis is carried out in each area of the embankment to estimate the

269 extent of the variation in erosion-induced fines contents. Soils are sieved in a dry condition. This is  
270 because the non-plastic sample, with a large grain size ratio of coarse to fine components, is easily  
271 separated. This test is conducted once per each divided element. For each test, the sieves are cleaned  
272 with a vibrator, an air duster gun, and a needle bar. Since the sieving was conducted in a dry  
273 condition, the possibility of the loss in fines during the sieving cannot be denied. However, as Silica  
274 sand No. 8, which is used as the erodible fines particles in this experiment, is classified as fine sand,  
275 the amount of loss is minimal. The samples are taken 24 h after the end of the seepage tests. At this  
276 time, the model ground is under partially saturated conditions and the shape of the model is  
277 maintained by suction. To avoid the collapse of the model, the steel box is tilted at 30° to the upright  
278 during the sample collection. In the sampling, a thin plate is penetrated perpendicular to the side face  
279 of the model. The work is conducted with great care as quickly as possible to prevent the drying of  
280 the soil (minimum time 5 h, maximum time 8 h). The number of sampling areas for the sieve  
281 analyses is given in Table 2. Since no previous studies have reported the detailed distribution of the  
282 fines fractions in the physical model, this is one of the features of the present study.

### 283 3. Results and Discussion

#### 284 3.1 *First permeation-induced change in spatial distribution of fines (Case St1)*

285 Fig. 5 shows the evolutions of the cumulative eroded soil mass and the variation in pore water  
286 pressure with time for *Case St1*. The left vertical axis is for the evolutions of the cumulative eroded  
287 soil mass, while the right one is for the variation in pore water pressure. The variations in pore water  
288 pressure are not directly linked to the water level. They depend on not only the hydrostatic pressure,  
289 but also the influence of the immediate fines distribution. From this figure, it can be seen that the  
290 pore water pressure increases with the increase in the water level at all the measurement points until  
291 around 0.2 h. After that, they show a peak value around an elapsed time of 0.2 h. Finally, they reach a  
292 nearly steady seepage condition.

293  
294 The initiation of fines erosion is observed almost as soon as the pore water pressure, located at the  
295 bottom of the toe (P4 in Fig. 3), starts rising. Major fines erosion takes place over a period of around  
296 0.15 h (540 s) after the detection of the eroded soil from the model. After that, the increment in  
297 eroded soil mass with time becomes small. These facts suggest that a relatively large amount of soil  
298 is eroded under the unsteady seepage condition, i.e., during the first permeation of water to the  
299 embankment.

300  
301 The distribution of changes in the fines contents, normalized by the initial value, is plotted in Fig. 6  
302 for *Case St1*. The changes in the spatial distribution of the fines are calculated by assuming that the  
303 initial fines content is the same in all parts of the model embankment before the seepage tests. In the  
304 figure, the observed phreatic surface before the end of the seepage tests is indicated by a solid line.

305

306 A decrease in fines is observed throughout the model, especially at the bottom of the foundation near  
307 the downstream boundary (Fig. 6). The majority of these changes in the spatial distribution of the  
308 fines may occur before reaching the nearly steady state. A lot of fines wash out during the first  
309 permeation and this may be attributed to the disappearance of suction due to the saturation and the  
310 reposition of fines by hydraulic force. The first arrival of seepage water may cause changes in the  
311 effective stress, resulting in small changes in the structure of the soil. A particle held in a stable  
312 position before wetting suffers hydraulic force, such as seepage force and buoyancy force, when the  
313 seepage water reaches the particle. Then, a movable particle initiates the migration or transportation.  
314 The initiation might depend on the particle size and/or the initial position in the void of the coarse  
315 skeleton. This particle migration or transportation leads to changes in the immediate local flow  
316 conditions and an infinitesimal collapse of the initial structure of the soil. As a result, fines reposition  
317 takes place. Fell et al. (2003) explained that the vulnerability to dam failure is greater on the first  
318 water filling or at the historic high reservoir water level. In other words, marked changes in hydraulic  
319 stability against seepage of an embankment occur during the wetting.

### 320 3.2 *Characteristics of erosion under the steady seepage flow*

321 Fig. 7 shows the evolutions of the cumulative eroded soil mass for *Cases St20, St24, and St48* and  
322 the discharge rate of water at the toe, with the exception of *Case St1*. The right vertical axis is for the  
323 normalized mass of erosion. The eroded soil ratio in Table 2 and the normalized mass of erosion in  
324 Figs. 7 and 12 are calculated by normalizing the cumulative eroded soil mass by the total fines (Silica  
325 sand No. 8) in the model before the seepage tests. In *Case St48*, the data are not collected  
326 continuously. The ending total eroded soil masses are as summarized in Table 2. As shown in Fig. 7,  
327 major fines erosion takes place in the early stage of the seepage tests (until around 1–4 h). In this  
328 period, the discharge rate is relatively large. After that, the erosion rates get smaller and the discharge  
329 rate also gradually decreases with time to 0.4–0.6 L/min.

330

331 Some discrepancy in the cumulative eroded soil mass exists, i.e., the eroded soil mass is relatively  
332 large in *Case St280* (see Table 2) and the discharged rate is also large in this case, compared with the  
333 other cases. The exact causes are unclear, but the authors infer the occurrence of a relatively strong  
334 flow between the sidewall and the soil in this case. However, as the spatial distributions of fines  
335 fractions in the middle cross section in this case show a coherent trend, compared with the other  
336 cases, this test result is also used to discuss the progress of suffusion in the following subsections.

337

338 The main cause of the fines erosion in the early stage of the seepage tests is attributed to the  
339 disappearance of suction due to water permeation and the reposition of fines by hydraulic force, as  
340 described above. After a certain elapsed time, the evolution of suffusion slowly continues under the  
341 nearly steady seepage conditions in the embankment, as described by Luo et al. (2012), for the

342 one-dimensional seepage tests, i.e., fine particles migration-pores clogging-pushing out clogging  
343 pores-fine particles remigration.

344

345 The distributions of the changes in the percentage of the fines contents normalized by the initial  
346 value are plotted in Fig. 8 for all the cases. After a certain elapsed time, it became difficult to observe  
347 the accurate phreatic surface for the wetting of the soil. Thus, the phreatic surface could not be  
348 observed except in the case of *Case St1*. Therefore, in the figure, the observed phreatic surface before  
349 the end of *Case St1* is indicated by a solid line to show the approximate position of the phreatic  
350 surface for each case. All the results show that the fines content decreases as a whole, especially for  
351 elements near the downstream boundary. A decrease in fines in the elements near the upstream  
352 boundary is also seen because of the absence of a supply of fines from the upstream. The following  
353 can be observed from the figure:

- 354 · In *Cases St24, St48, and St280* (Fig. 8(b)–(d)), a regressive decrease in fines along the phreatic  
355 surface is observed from the middle of the foundation near the downstream boundary.
- 356 · In *Case St20*, an increase in the fines content is observed in some elements.
- 357 · In *Case St48*, although the seepage time for *Case St48* is longer than that for *Cases St20 and St24*,  
358 the cumulative eroded soil mass for *Case St48* is relatively small.
- 359 · In *Case St280*, the magnitude of change in the spatial distribution of fines is large compared with  
360 that in the other cases. It also shows an increase in fines in the foundation, horizontally 30 mm  
361 and 280 mm in distance from the toe of the slope.

362

363 As shown in Fig. 7, the erosion rate correlates to the flow rate. In other words, the transportation of  
364 particles correlates with the hydraulic conductivity of the entire embankment. During the steady  
365 seepage, the erosion rates get smaller and the discharge rate also gradually decreases with time.  
366 Previous one-directional seepage tests showed a similar trend, i.e., a decrease in hydraulic  
367 conductivity with elapsed time (e.g., Lafleur, 1999; Bendahmane et al., 2008; Marot et al., 2012), as  
368 can be observed in Fig. 7. The decrease in hydraulic conductivity may be the result of the  
369 suffusion-induced clogging in the soil specimen. Lafleur (1999) showed that the variations in general  
370 hydraulic conductivity of a specimen depend on the spatial distribution of fines in the specimens in  
371 their interpretation of downward filtration tests on geotextiles and cohesionless soils. If this  
372 interpretation is applied to the present study, it can be said that the permeability of the whole  
373 embankment depends on the spatial distribution of the fines fraction in the embankment.

374

375 To understand the progress of suffusion in the embankment under a steady seepage flow, an attempt  
376 is made to visualize the changes in the fines content distribution using the tests with different seepage  
377 times. Assuming all initial test conditions and erosion processes are the same, the tests are arranged  
378 in ascending order of the seepage time or cumulative eroded mass. To eliminate the changes in fines  
379 content during the transient stage, i.e., before the seepage flow becomes stable, the distributions of

380 the changes in the incremental percentage in the fines content, making Case St1 a reference, are  
381 plotted in Fig. 9.

382

383 It is not very clear, but a decrease in fines is observed in the slope zone and in the upper half of the  
384 foundation, while an increase in fines can be seen in the bottom half of the foundation over one or  
385 two days of steady seepage (Fig. 9 (a)–(c)). This contrast becomes clearer with the elapse time. In  
386 *Case St280*, many fines are eroded out (it should be noted, however, that the discharge rate in this  
387 case is larger than in the other cases) and a large decrease in fines occurred in Area B near the toe and  
388 in Area C near the phreatic surface in the slope zone (Fig. 9(d)).

389

390 An increase in fines can be observed at the bottom of the foundation around horizontally 0–70 mm  
391 and 315–385 mm in distance from the toe of the slope under a steady seepage flow. These areas of  
392 increased fines develop in the horizontal direction with time. As the seepage flow is mostly  
393 horizontal at the foundation, leftward horizontal migration of the fines is expected. However, the  
394 decreasing rate at element A is relatively small, compared with the increasing rate at the further  
395 downstream locations at the bottom of the foundation. A possible explanation for this is the migration  
396 of fines in the other directions. In other words, the eroded fines move not only by the seepage flow,  
397 but also by the gravitational vertical force, and deposit in the foundation. This local concentration of  
398 fines in the embankment may cause a decrease in the permeability of the whole embankment, as  
399 shown in Fig. 7, which is consistent with the interpretation of the elemental tests by Lafleur (1999).

### 400 3.3 *Effect of repeated permeation*

401 To investigate the characteristics of erosion in a regular pattern of the rising and falling phreatic  
402 surface, focus is placed on the results of *Case St96RS4*, which show a well-controlled boundary  
403 water level and regular repeated permeations. Fig. 10 shows evolutions of the cumulative eroded soil  
404 mass at each of the seepage periods for *Case St96RS4*. This result shows that the erosion of fines  
405 occurs mostly during the first seepage period. From the second period, the eroded mass decreases. In  
406 all seepage periods, major fines erosion takes place in the early stage (until around 5 h). The  
407 measured cumulative eroded soil mass at the beginning of each seepage period shows a negative  
408 value, as presented in Fig. 10. The exact causes are unclear, but the authors infer that the fluctuation  
409 in the water surface in the plastic container shown in Fig. 3(b) is due to some trouble leading to a  
410 variation in measurement values.

411

412 Changes in the discharge rate of the water at the toe, for each seepage period in *Case St96RS4*, are  
413 shown in Fig. 11. In this figure, it is observed that the discharge rate of water increases slightly from  
414 the third seepage period. This means that the permeability of the whole embankment increases with  
415 the increasing times of repeated permeation.

416

417 Fig. 12 shows the evolutions of the cumulative eroded soil mass for *Cases St280* and *St280RS40*. In  
418 *Case St280RS40*, the discharge rate of water is not measured. However, according to the evolutions  
419 of the cumulative eroded soil mass at the first seepage period for *Cases St280* and *St280RS40*, the  
420 discharge rate of water for *Case St280RS40* is expected to be the same level.

421

422 The distribution of the changes in the percentage of the fines contents is plotted in Fig. 13 for *Cases*  
423 *St96RS4*, *St96RS8*, and *St280RS40*. The following trend in the changes in the spatial distribution of  
424 fines can be understood from each figure:

- 425 · In *Case St96RS4*, a decrease in fines can be seen from the middle of the foundation near the  
426 downstream boundary (Fig. 13(a)).
- 427 · In *Case St96RS8*, a decrease in fines can be confirmed from the middle of the foundation near  
428 the downstream boundary and the upper part of the slope zone (Fig. 13(b)). A high concentration  
429 of fines is observed around the middle of the slope zone below the phreatic surface.
- 430 · In *Case St280RS40*, a decrease in fines can be observed from the middle of the foundation near  
431 the downstream boundary to the lower section of the crown. The increase in fines at the  
432 foundation zone is larger and more extensive than for the other cases (Fig. 13(c)).

433

434 The major fines erosion in the early stage of each seepage period, shown in Fig. 10, is attributed to  
435 the disappearance of suction due to the saturation and the reposition of fines by hydraulic force, as  
436 described in the previous subsections.

437

438 To understand the effect of the repeated permeations on the spatial distribution of fines, the results of  
439 sieve analyses for *Cases St280* and *St280RS40* are compared. The distribution of the changes in the  
440 incremental percentage of the fines content, making *Case St280* a reference, is plotted in Fig. 14 for  
441 *Case St280RS40*. From the figure, the clear boundary D–D' that separates the areas of increase and  
442 decrease of fines is seen. This indicates that a number of fines are transported from decreased  
443 elements to elements located just below or obliquely downward due to repeated permeations. In  
444 other words, repeated permeations lead to the prominent vertical transportation of fines around the  
445 boundary between the slope zone and the foundation zone. The causes of this formation of the clear  
446 boundary at D–D' remain unknown, but it can be said that the drawdown between cycles allows the  
447 transported fines to settle and this is one of the reasons for the marked increase in fines in the  
448 foundation zone.

#### 449 4. Conclusions

450 In this paper, a series of physical model tests on seepage- induced suffusion in a homogeneous  
451 embankment has been conducted. Binary mixtures, consisting of two Silica sands (Silica sands Nos.  
452 3 and 8) with different dominant particle sizes, have been used for the model embankment. The  
453 seepage-induced temporal and spatial variations in the fines contents in the embankment have been

454 examined through sieve analyses on subdivided areas of the model embankment after seepage testing,  
455 and the following conclusions are drawn:

- 456 1. Seepage-induced suffusion in an embankment can be reproduced with a small-scale loosely  
457 compacted levee model in the laboratory.
- 458 2. Sieve analyses in each area of the embankment can help to successfully observe the spatial  
459 distribution of fines within the model embankment.
- 460 3. Under the transient seepage condition in the first permeation, major fines erosion takes place due  
461 to the rising phreatic surface. The disappearance of suction and the transportation of fines with  
462 the seepage flow change the distribution of the fines content in the embankment.
- 463 4. After a certain elapsed time, suffusion backwardly develops along the phreatic surface from  
464 downstream in the embankment. Below the phreatic surface, the erodible fines not only move  
465 laterally by the seepage flow, but also vertically due to the gravitational force, and are deposited  
466 in the foundation. This deposition of the fines results in the expansion of the fine-rich region in  
467 the foundation and causes a decrease in the permeability of the whole embankment. In addition,  
468 it has been confirmed that repeated permeations lead to the prominent vertical transportation of  
469 fines from the slope zone to the foundation zone.

470

#### 471 **Acknowledgements**

472 This work was supported by JSPS KAKENHI, Grant number 25420498.

473

#### 474 **References**

- 475 Beguin, R., Fry, J. J., Picault, C., Courivaud, J. R., Faure, Y. H., Philippe, P., 2012. Control of the risk  
476 of dike failure caused by contact erosion. In: Proceedings of 6th International Conference on  
477 Scour and Erosion, Paris, pp. 1551–1558.
- 478 Bendahmane, F., Marot, D., Alexis, A., 2008. Experimental parametric study of suffusion and  
479 backward erosion. *J. Geotech. Geoenviron. Eng.* 134 (1), 57–67.
- 480 Chang, D.S., Zhang, L.M., 2013. Extended internal stability criteria for soils under seepage. *Soils*  
481 *Found.* 53 (4), 569–583.
- 482 Cividini, A., Bonomi, B., Vignati, G.C., Gioda, G., 2009. Seepage-induced erosion in granular soil  
483 and consequent settlements. *Int. J. Geomech.* 9 (4), 187–194.
- 484 Cividini, A., Gioda, G., 2004. Finite-element approach to the erosion and transport of fine particles in  
485 granular soils. *Int. J. Geomech.* 4 (3), 191–198.
- 486 Fell, R., Fry, J.J., 2013. State of the art on the likelihood of internal erosion of dams and levees by  
487 means of testing. In: Bonelli, S. (Ed.), *Erosion in Geomechanics Applied to Dams and Levees*.  
488 ISTE-Wiley, London, UK, pp. 1–99 Chapter 1.
- 489 Fell, R., Wan, C.F., Cyganiewicz, J., Foster, M., 2003. Time for development of internal erosion and  
490 piping in embankment dams. *J. Geotech. Geoenviron. Eng.* 129 (4), 307–314.
- 491 Foster, M., Fell, R., 1999. A framework for estimating the probability of failure of embankment dams

492 by internal erosion and piping using event tree methods. University of New South Wales, Sidney  
493 UNICIV reports.

494 Foster, M., Fell, R., 2001. Assessing embankment dam filters that do not satisfy design criteria. *J.*  
495 *Geotech. Geoenviron. Eng.* 127 (5), 398–407.

496 Foster, M., Fell, R., Spannagle, M., 2000. The statistics of embankment dam failures and accidents.  
497 *Can. Geotech. J.* 37 (5), 1000–1024.

498 Fry, J.J., 2012. Introduction to the process of internal erosion in hydraulic structures: embankment  
499 dams and dikes. In: Bonelli, S. (Ed.), *Erosion of Geomaterials*. ISTE-Wiley, London, UK, pp. 1–  
500 36 Chapter 1.

501 Fry, J.J., Vogel, A., Royet, P., Courivaud, J.R., 2012. Dam failures by erosion: lessons from ERINOH  
502 data bases. In: *Proceedings of 6th International Conference on Scour and Erosion*, Paris, pp. 273–  
503 280.

504 Honjo, Y., Haque, M. A., and Tsai, K. A., 1996. Self-filtration behavior of broadly and gap graded  
505 cohesionless soils. In: *Proceedings of 2nd International Conference on Geofilters*, Montreal, pp.  
506 227–236.

507 Ke, L., Takahashi, A., 2012. Strength reduction of cohesionless soil due to internal erosion induced  
508 by one-dimensional upward seepage flow. *Soils Found.* 52 (4), 698–711.

509 Ke, L., Takahashi, A., 2014. Experimental investigations on suffusion characteristics and its  
510 mechanical consequences on saturated cohesionless soil. *Soils Found.* 54 (4), 713–730.

511 Kenney, T.C., Lau, D., 1985. Internal stability of granular filters. *Can. Geotech. J.* 22 (2), 215–225.

512 Khomenko, V.P., 2006. Suffosion hazard: Today's and tomorrow's problem for cities. In: *Proceedings*  
513 *of the 10th IAEG International Congress*, Nottingham, pp. 1–8.

514 Kuwano, R., Kohata, Y., Sato, M., 2012. A case study of ground cave-in due to large scale subsurface  
515 erosion in old land fill. In: *Proceedings of 6th International Conference on Scour and Erosion*,  
516 Paris, pp. 265–271.

517 Ladd, R.S., 1978. Preparing test specimens using undercompaction. *Geotech. Test. J.* 1 (1), 16–23.

518 Lafleur, J., 1999. Selection of geotextiles to filter broadly graded cohesionless soils. *Geotext.*  
519 *Geomembr.* 17 (5–6), 299–312.

520 Li, M., Fannin, R.J., 2008. Comparison of two criteria for internal stability of granular soil. *Can.*  
521 *Geotech. J.* 45 (9), 1303–1309.

522 Lindow, N., Fox, G., Evans, R., 2009. Seepage erosion in layered stream bank material. *Earth Surf.*  
523 *Process. Landf.* 34, 1693–1701.

524 Luo, Y., Qiao, L., Liu, X., Zhan, M., Sheng, J., 2012. Hydro-mechanical experiments on suffusion  
525 under long-term large hydraulic heads. *Nat. Hazards* 65 (3), 1361–1377.

526 Marot, D., Bendahmane, F., Nguyen, H.H., 2012. Influence of angularity of coarse fraction grains on  
527 internal erosion process. In: *Proceedings of 6th International Conference on Scour and Erosion*,  
528 Paris, pp. 887–894.

529 Moffat, R., Fannin, R.J., 2011. A hydromechanical relation governing internal stability of

530 cohesionless soil. *Can. Geotech. J.* 48 (3), 413–424.

531 Moffat, R., Fannin, R.J., Garner, S.J., 2011. Spatial and temporal progression of internal erosion in  
532 cohesionless soil. *Can. Geotech. J.* 48 (3), 399–412.

533 Moraci, N., Mandaglio, M.C., Ielo, D., 2014. Analysis of the internal stability of granular soils  
534 using different methods. *Can. Geotech. J.* 51 (9), 1063–1072.

535 Perzmaier, S., Muckenthaler, P., Koelewijn, A.R., 2007. Hydraulic criteria for internal erosion in  
536 cohesionless soil. In: Fell, R., Fry, J.J. (Eds.), *Internal Erosion of Dams and Their Foundations*.  
537 Taylor & Francis Group, London, UK, pp. 179–190.

538 Richards, K.S., Reddy, K.R., 2007. Critical appraisal of piping phenomena in earth dams. *Bull. Eng.*  
539 *Geol. Environ.* 66 (4), 381–402.

540 Richards, K.S., Reddy, K.R., 2012. Experimental investigation of initiation of backward erosion  
541 piping in soils. *Géotechnique* 62 (10), 933–942.

542 Richards, K.S., Reddy, K.R., 2014. Kinetic Energy Method for predicting initiation of backward  
543 erosion in earthen dams and levees. *Environ. Eng. Geosci.* 20 (1), 85–97.

544 Saito, Y., Kuwano, R., Sasaki, T., 2012. The model tests on a permeability of ground against repeated  
545 process of seepage. In: *Proceedings of the 47th Japan National Conference on Geotechnical*  
546 *Engineering*, Hachinohe, pp. 903–904. (In Japanese).

547 Skempton, A.W., Brogan, J.M., 1994. Experiments on piping in sandy gravels. *Géotechnique* 44 (3),  
548 449–460.

549 Sterpi, D., 2003. Effects of the erosion and transport of fine particles due to seepage flow. *Int. J.*  
550 *Geomech.* 3 (1), 111–122.

551 Terzaghi, K., 1939. Soil mechanics: a new chapter in engineering science. *J. Inst. Civil Eng.* 12 (7),  
552 106–142.

553 Tomlinson, S.S., Vaid, Y.P., 2000. Seepage forces and confining pressure effects on piping erosion.  
554 *Can. Geotech. J.* 37 (1), 1–13.

555 Uzuoka, R., Ichiyama, T., Mori, T., Kazama, M., 2012. Hydro-mechanical analysis of internal  
556 erosion with mass exchange between solid and water. In: *Proceedings of 6th International*  
557 *Conference on Scour and Erosion*, Paris, pp. 655–662.

558 Wan, C., Fell, R., 2008. Assessing the potential of internal instability and suffusion in embankment  
559 dams and their foundations. *J. Geotech. Geoenviron. Eng.* 134 (3), 401–407.

560 Zhang, X., Dong, J., Huang, Z., Nie, X., Wong, H., Wang, J.X., 2014. Study of soil structures  
561 strength and stiffness loss based on thermodynamics and continuum mechanics. *Environ. Earth*  
562 *Sci.*

563 Zhang, X.S., Wong, H., Leo, C.J., Bui, T.A., Wang, J.X., Sun, W.H., Huang, Z.Q., 2013. A  
564 thermodynamics-based model on the internal erosion of earth structures. *Geotech. Geol. Eng.* 31  
565 (2), 479–492.

566

567 Table 1 Physical properties of tested soils

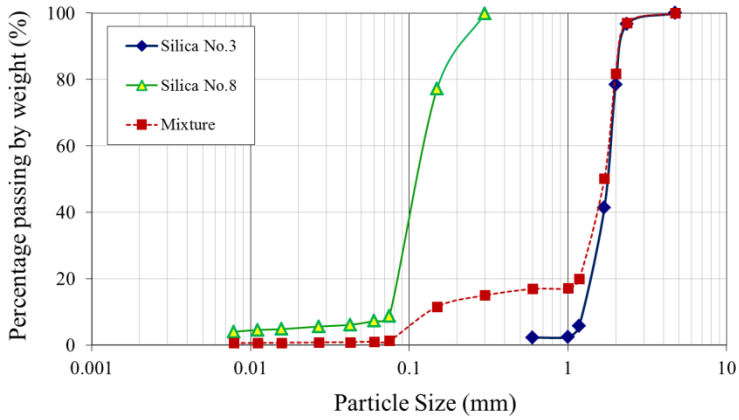
Physical property	Silica sand No. 3 (Coarse fraction)	Silica sand No. 8 (Fines)	Mixture
Specific gravity, $G_s$	2.645	2.645	2.645
Fines content, $FC$ (%)	—	—	15
Maximum void ratio, $e_{\max}$	0.94	1.33	0.79
Minimum void ratio, $e_{\min}$	0.65	0.7	0.53
Median particle size $D_{50}$ (mm)	1.76	0.16	1.78
Effective particle size $D_{10}$ (mm)	1.37	0.087	0.138
Uniformity coefficient, $C_u$	1.5	1.7	13
Curvature coefficient, $C_c$	1.1	0.96	7.9
Grain Description	Sub-rounded ~ Sub-angular		

568

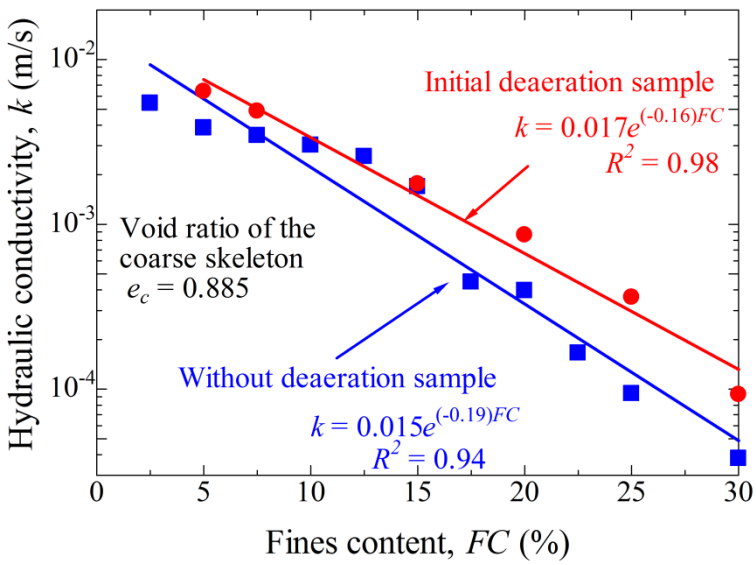
569 Table 2 Test cases of seepage testing

Case	Dry density ( $Mg/m^3$ )	Seepage time (hr)	Repeat count of supply and drainage	Number of sampling areas	Cumulative eroded soil mass (g)	Eroded soil ratio (%)
<i>St1</i>	1.559	0.55	1	48	22.77	0.764
<i>St20</i>	1.562	20	1	48	32.37	1.085
<i>St24</i>	1.560	24	1	48×3	34.88	1.169
<i>St48</i>	1.567	48	1	66	28.03	0.913
<i>St280</i>	1.560	280	1	45	154.67	5.190
<i>St96RS4</i>	1.560	96	4	48	44.55	1.495
<i>St96RS8</i>	1.560	96	8	95	43.11	1.447
<i>St280RS40</i>	1.559	280	40	47	234.82	7.885

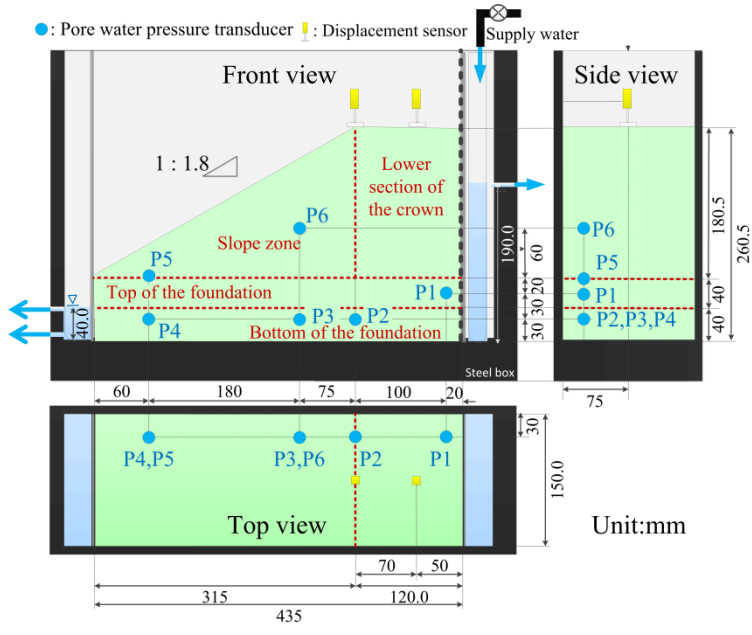
570



571  
 572 Fig.1. Grain size distribution curves of silica sands and their mixture  
 573

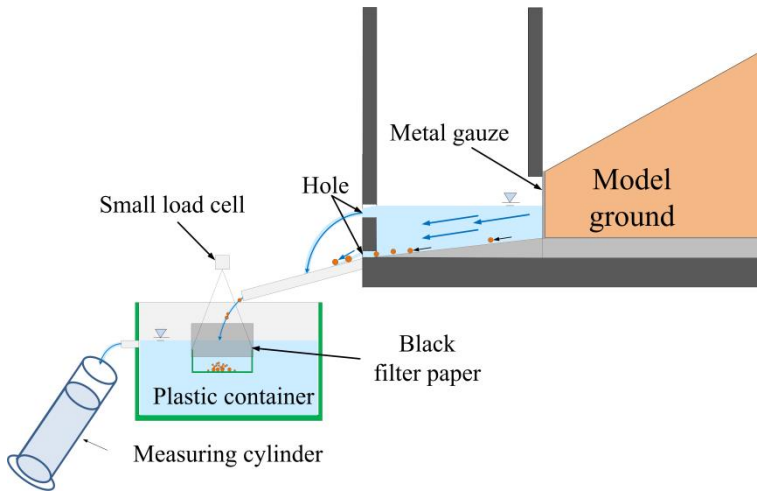


574  
 575 Fig.2. Relationships between fines content and permeability under constant void ratio of coarse  
 576 skeleton  
 577



578

a)

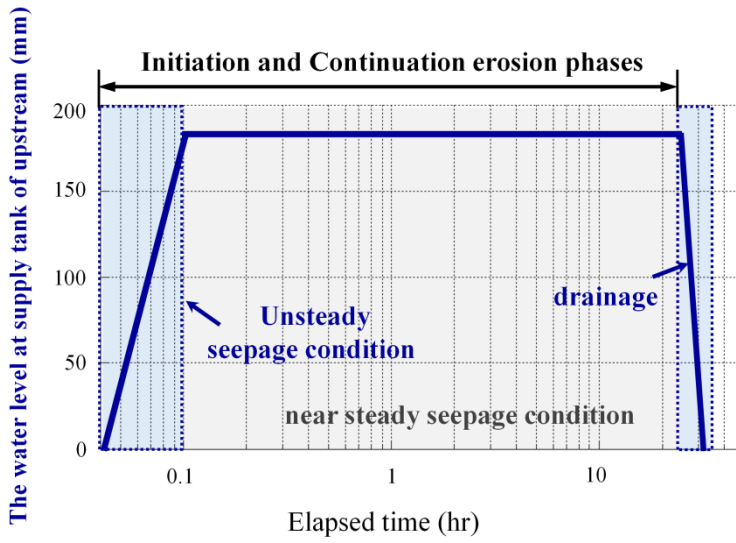


579

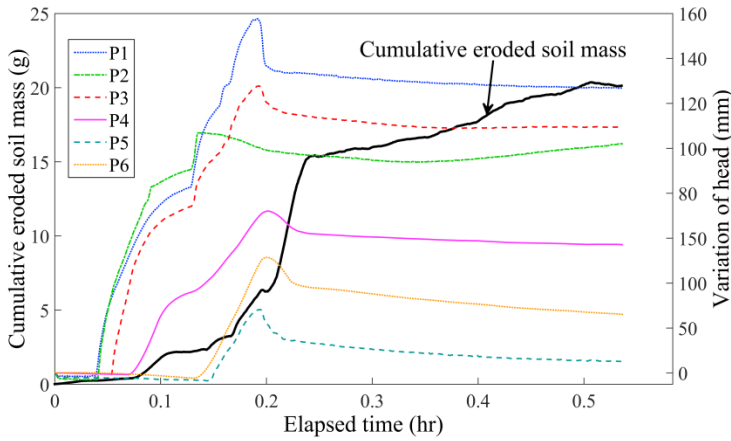
b)

580 Fig. 3. Schematic diagram of experimental system, (a) physical model, (b) Sampling on eroded  
 581 fines

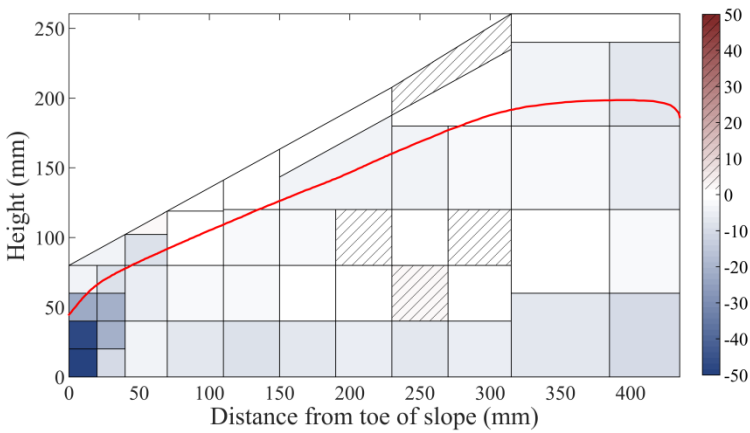
582



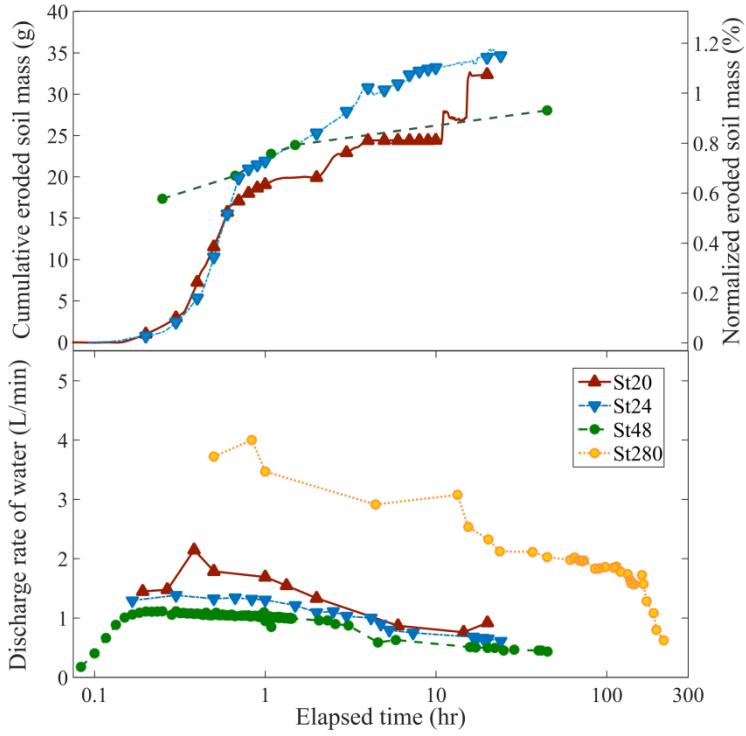
583  
 584 Fig. 4. Conceptual diagram of controlled water level at water supply tank  
 585



586  
 587 Fig. 5. Evolutions of cumulative eroded soil mass and variation of pore water pressure for *Case St1*  
 588



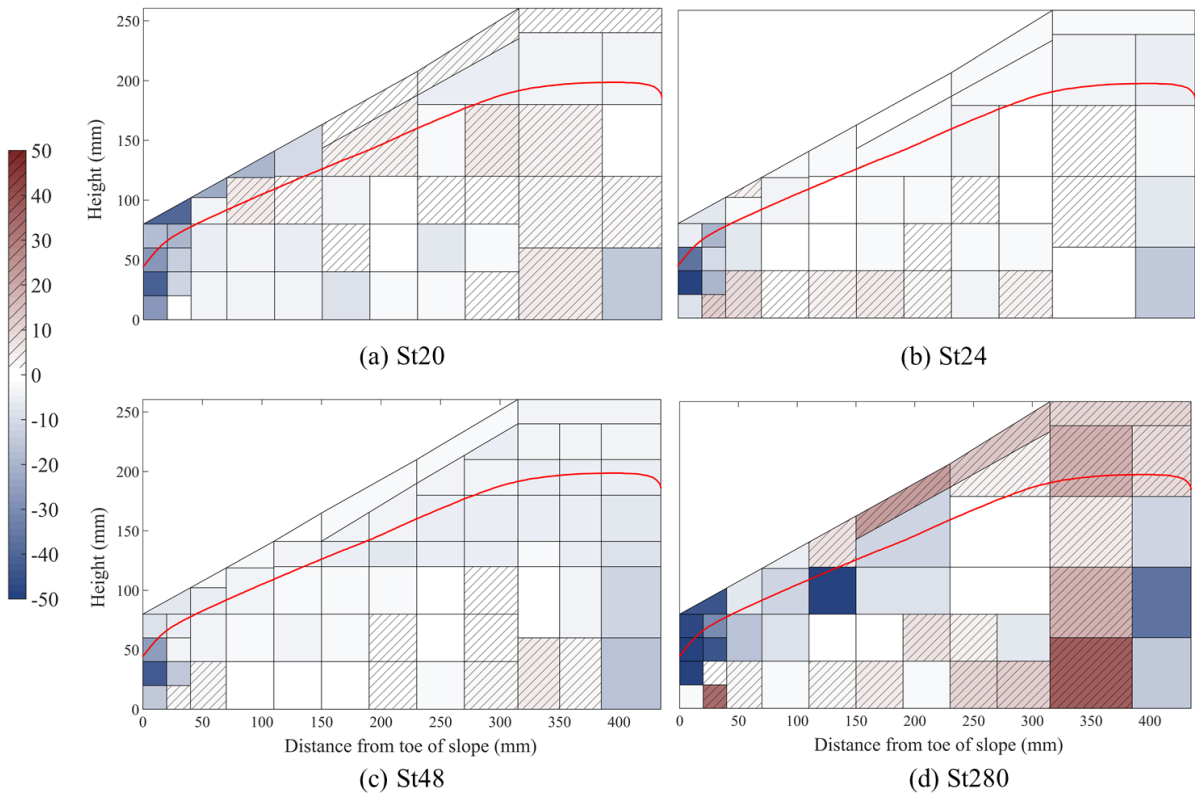
589  
 590 Fig. 6. Distribution of percentage change in fines content for *Case St1*  
 591



592

593 Fig. 7. Evolutions of cumulative eroded soil mass for Cases *St20*, *St24* and *St48* and evolutions of  
 594 discharge rate of water for Cases *St20*, *St24*, *St48* and *St280*

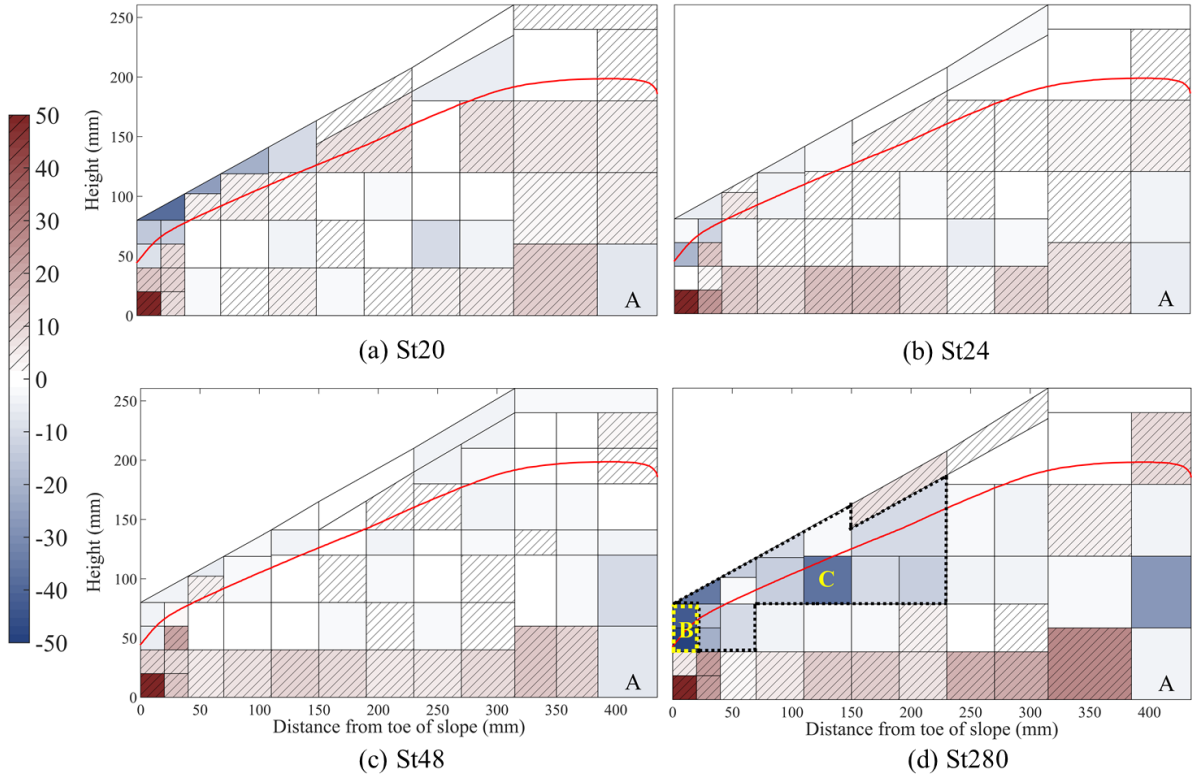
595



596

597 Fig. 8. Distributions of percentage change in fines content for Cases *St20*, *St24*, *St48* and *St280*

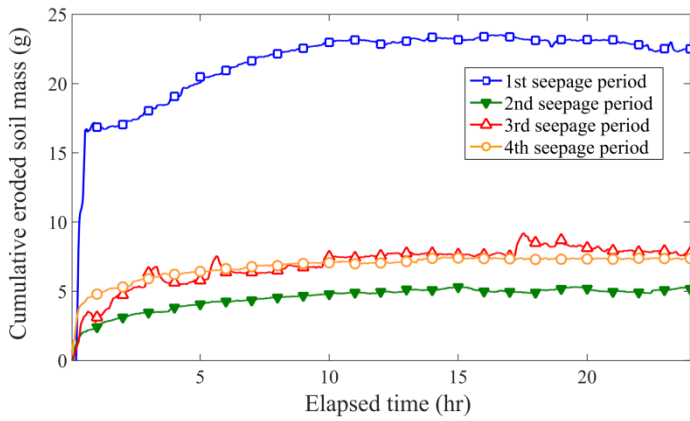
598



599

600 Fig. 9. Distributions of incremental percentage change in fines content by making Case St1 as a  
 601 reference, (a) *Case St20* (20 hours), (b) *Case St24* (24 hours), (c) *Case St48* (48 hours), (d) *Case St*  
 602 *280* (280 hours)

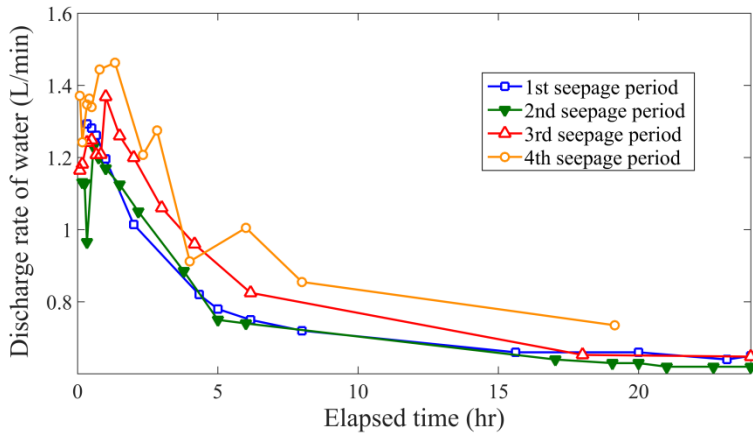
603



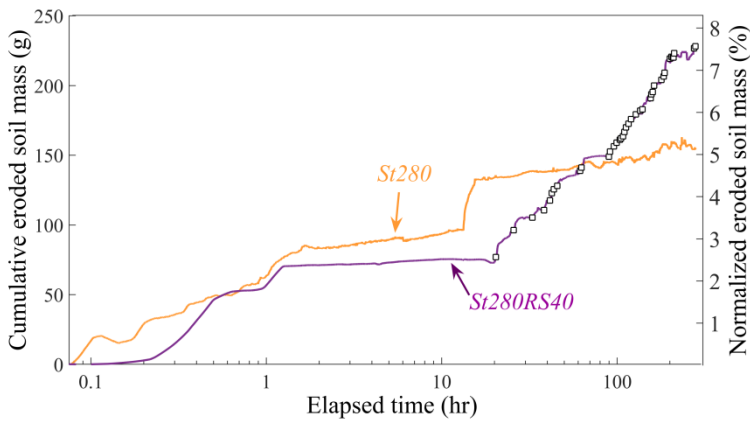
604

605 Fig. 10. Evolutions of cumulative eroded soil mass at each seepage period for *Case St96RS4*

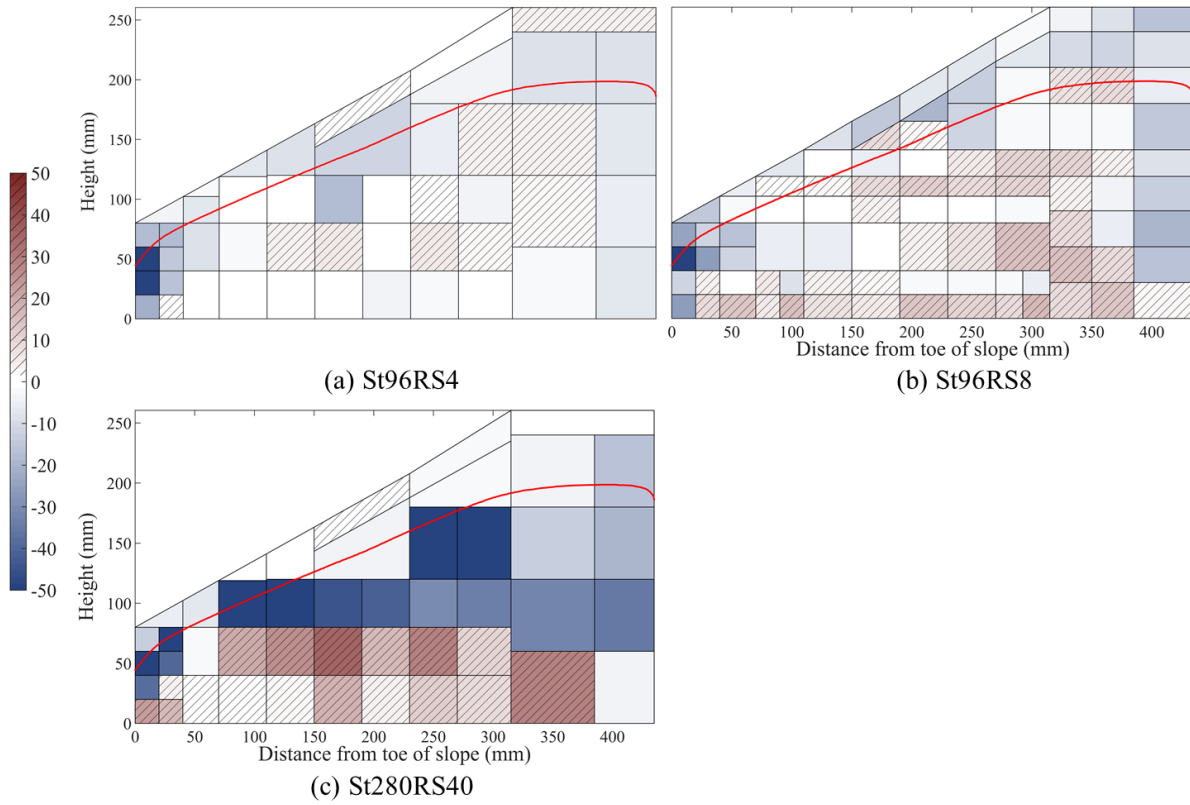
606



607  
 608 Fig. 11. Evolutions of discharge rate of water for *Case St96RS4*  
 609



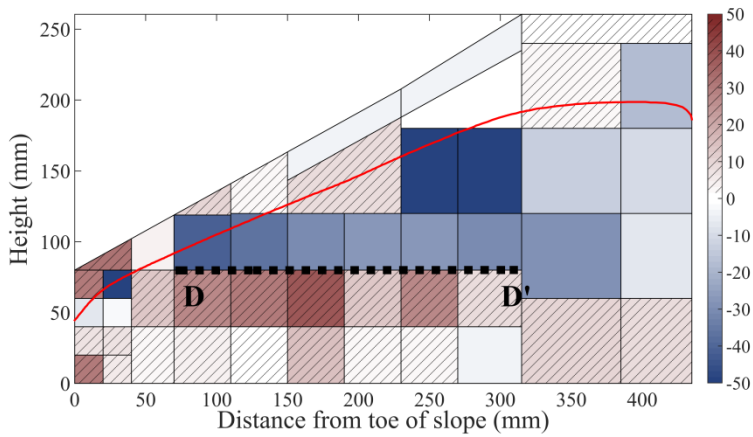
610  
 611 Fig. 12. Evolutions of cumulative eroded soil mass for *Cases St280* and *St280RS40*  
 612



613

614 Fig. 13. Distributions of percentage change in fines content for *Cases St96RS4, St96RS8 and*  
 615 *St280RS40*

616



617

618 Fig. 14. Distribution of incremental percentage change in fines content by making *Case St280* as a  
 619 reference for *Case St280RS40*